NASA Technical Memorandum 104426

IN-34

37382

P-27

Parched Elastohydrodynamic Lubrication: Instrumentation and Procedure

Bryan Schritz
Case Western Reserve University
Cleveland, Ohio

Wiliam R. Jones, Jr.
Lewis Research Center
Cleveland, Ohio

Joseph Prahl and Ralph Jansen
Case Western Reserve University
Cleveland, Ohio

NASA

PARCHED ELASTOHYDRODYNAMIC LUBRICATION:

INSTRUMENTATION AND PROCEDURE

Bryan Schritz
Case Western Reserve University
Cleveland, Ohio 44106

William R. Jones, Jr.
National Aeronautics and Space Administration
Lewis Research Center
Cleveland, Ohio 44135

Joseph Prahl and Ralph Jansen
Case Western Reserve University
Cleveland, Ohio 44106

SUMMARY

A counter rotating bearing rig has been designed and constructed to study transient elastohydrodynamic lubrication phenomena. This paper describes new instrumentation and documents test procedures. Ball and race speed measurement systems and the capacitance (film thickness) measurement system were upgraded. Methods for measuring bearing torque and race temperatures were implemented.

INTRODUCTION

Starvation theory, a subdivision of elastohydrodynamic lubrication (EHL), was described a number of years ago (ref. 1). It relates to the situation occurring in ball bearings having a restricted oil supply in which pressure build-up in the inlet is inhibited resulting in a film thickness thinner than calculated by classical EHL theory (ref. 2).

Starvation theory fails to adequately describe instrument ball bearing behavior. Another subdivision of EHL, "parched" describes this behavior where there is no free bulk oil in the system (ref. 3). The lubricant films are so thin that they are immobile outside the Hertzian contact zone. This regime is of practical importance since parched bearings require the least driving torque and also have the most precisely defined spin axis.

The lubricant inside a Hertzian contact is not immobile and is eventually squeezed out resulting in long-term film thinning transients (refs. 4 and 5), which leads to film failure and subsequently bearing failure. In order to prevent failure, make-up oil must be added to balance the loss due to cross flow.

As film thinning occurs, shear rate increases and mechanical shear energy is then concentrated in smaller and smaller Hertzian volumes. At some point in this process, the shear energy causes irreversible chemical changes in the lubricant, resulting in degradation and/or polymerization (ref. 6).

For retainerless bearings operating at low contact stresses, it has been suggested that a beneficial in-situ polymeric film is produced which yields a

geometrically perfect, plastic ball separator in just the right location
(ref. 7). This is particularly important since elimination of the retainer in
a bearing precludes any retainer instability problems which commonly occur in
gyroscope bearings (ref. 8).

To study these concepts, a Transient Elastohydrodynamic Lubrication
Apparatus (TEHL) was initially designed and constructed by Kingsbury (ref. 3).
Later, modifications by Hunter (ref. 9) allowed for calculation of film thick-
ness from capacitance measurements.

The objective of this paper is to describe several new modifications to
the TEHL apparatus and to completely document its operation. The ball and
race speed measurement systems and the capacitance measurement system were
upgraded. Methods for measuring bearing torque and race temperature were
implemented. Finally, a computer data acquisition system was installed.

TEHL APPARATUS - BASIC OPERATION

The overall apparatus is shown in figure 1. It consists of the TEHL
apparatus itself, inner and outer race drive motors (the latter containing a
torque sensor) and a loading mechanism. The TEHL apparatus appears in
figure 2. The upper bearing is the test bearing. The outer race of this
bearing is driven by a synchronous hysteresis motor through a toothed belt
drive. A keyed bushing is press fit into the inner race. The load ring is
keyed into the bushing and a spindle, which is driven by a second synchronous
motor through another toothed belt drive. This allows the bearing to be run
in a counter - rotating mode (the races spin in opposite directions such that
the ball complement is stationary). The bearing is loaded with a deadweight
axially through the load ring and the central load shaft that extends down
through the spindle (fig. 3). The four lower bearings provide support and
alignment.

Ball-race coupling is followed by measuring the basic speed ratio (BSR)
of the bearing (ref. 10). BSR is defined as:

$$BSR = \frac{\Omega_b}{\Omega_o + \Omega_i} \tag{1}$$

where Ω_b is the ball spin rate and Ω_i and Ω_o are the inner and outer
race spin rates, respectively (algebraic sign defined as shown in fig. 4).

BEARING CAPACITANCE, FILM THICKNESS, AND CONDUCTIVITY

The bearing capacitance measurement system consists of a Hewlett-Packard
4267A (inductance-capacitance-impedance) LCZ meter, interfaced with an IBM
compatible personal computer through an IEEE-488 interface bus. The LCZ meter
is connected to the bearing by four coaxial cables. Two of these cables sup-
ply a known alternating current across the bearing and two carry the voltage
that is developed across the bearing as a result of this current back to the
LCZ meter as shown in figure 5. Measurements of the amplitude and phase shift
(relative to the supply current) of the returned voltage are made by the

instrument, and the total impedance across the bearing is calculated. The impedance is resolved into an effective parallel capacitance and conductance, which are the actual values displayed by the meter. The average contact film thickness is then calculated from the capacitance readings by a computer program from a method developed by Dyson et al. (ref. 12) for cylinders but successfully applied to ball bearings by Allen, et al. (ref. 13).

Actual electrical connections to the bearings are made through two sets of slip rings (fig. 5). The first set carries all four wires from the stationary lab reference frame to the rotating outer housing. Two wires (one current supply and one voltage sense) are attached to a screw, which in turn, is tightened against the outer bearing race. The other two wires pass through the second slip ring assembly (whose stator rotates with the outer housing) to the load ring, where they are attached by a screw. The load ring makes direct metal contact with the inner race, completing the circuit. The whole apparatus is electrically isolated from ground (except for a 5 MΩ bleed-off resistor, which drains away static build-up). Isolation from ground is necessary for proper operation of the LCZ meter. Typical capacitance readings are on the order of 500 pF, with an accuracy of about ±2 pF, and conductance readings are in the 1 μs (microsiemens) range, accurate to ±0.1 μs.

Stray capacitance and conductance values are measured by breaking the circuit and by backing out the outer race contact screw, and then taking readings from the meter. These stray background readings are then subtracted from the values read from the LCZ meter.

BALL AND RACE SPEEDS

The ball and race speed measuring circuit is more complicated than the capacitance measuring circuit (fig. 6). It is also considerably more accurate, on the order of ±0.001 percent. This is important in the calculation of the rate of slip in the ball-race contacts. There are three basic sections to this system: the race speed measurement, the ball spin measurement, and the ball complement position controller.

RACE SPEED

The races are driven by synchronous motors through timing belt and pulley arrangements. To determine the race speed, it is sufficient to measure the drive frequency of the motors, and divide by a constant (in this case, the integer 4). The constant is determined by the pole arrangement of the motors, and the ratio of the number of teeth on the driving pulley to the number on the driven pulley. The signals from monitor outputs on each of the variable frequency power supplies used to drive the motors are fed into a pair of counters. The counters measure the period of the signals and transmit the information to the computer through the IEEE-488 interface bus.

BALL SPIN RATE

To measure the ball spin rate, one of the bearing balls is slightly magnetized. A pick-up coil, made of 1000 turns of number 34 A.W.G. magnet

3

wire wound on a laminated iron core, is positioned near the magnetized ball. (The ball is stationary in space because of the counter-rotating mode of bearing operation, as noted previously.) The output signal from the coil is on the order of several millivolts, and has significant components of many frequencies related to the apparatus and the instrumentation. This signal is first boosted by a preamp with a gain of around 100, and a low pass filter with a roll-off to 12 dB/octave past the -3 dB point of 1000 Hz. (Ball spin rates are typically 200 to 300 Hz.) The signal is then sent through a series of three sharp (Q = 50 to 100) Deliyannis band pass filters (ref. 11), an automatic gain control, a differentiator, and then a zero-crossing detector. The output is a square wave of precisely the same frequency as the ball spin rate. This is then sent to a counter, which measures the period of the wave, and sends the information to the computer through the IEEE-488 interface bus, just like the race speed counters.

BALL COMPLEMENT POSITION CONTROLLER

An important part of the speed measuring circuitry is the ball complement position controller. In order for the ball spin rate to be accurately measured under the assumption of zero ball complement orbital rate, the complement velocity must be exactly zero. The controller makes minute adjustments to the inner race speed to keep the ball complement stationary during the course of the test run.

A second coil, identical to the one used in the ball spin rate measurement circuit, is placed near the bearing, about 45° away from the first coil During a test run, the magnetized ball sits between two coils, generating an EMF in each of them. If the ball is exactly halfway between them, the magnitude of the EMF generated at the ball spin frequency will be the same in each coil. If the ball begins to move toward one coil, the EMF generated in that coil will increase in magnitude, while that in the other coil will decrease. The difference in magnitude gives a measurement of the magnetized ball's position between the two coils.

The second coil is fed through a preamp identical to the one used with the first coil. The output signals from the two preamps are then fed into the controller box (fig. 6). Inside the box, both signals pass through identical parallel Deliyannis filter sections, and then rectifier sections, to obtain the two amplitudes. The difference in these two amplitudes is sent through a buffer/damper section and then into a PID controller. The output from the controller may go through an invertor, if necessary, to get the proper controller action, depending on the direction of motor rotation. The output is then added to a dc bias voltage to form the main control signal, which is output from the controller box. This control signal is sent into the voltage controlled oscillator input of a signal generator, which in turn is used to synchronize the inner race drive motor power supply. Thus, any disturbances in the position of the ball complement results in an adjustment of the inner race rotation rate to return the ball complement to its original position.

4

TORQUE AND TEMPERATURE MEASUREMENTS

In setting up bearing torque measurement system consideration had to be given to not disturb the other measuring apparatus. In order to accomplish this, it was necessary to use a somewhat unconventional method of torque measurement.

It is relatively easy to measure the torque required by the test bearing and the upper support bearing together: Simply measure the torque output of the motor, multiply by the ratio of the number of teeth on the driven pulley to the number on the driver pulley, and subtract losses due to windage, and slip rings. Because of the mechanical coupling between those two bearings, it is necessary to consider thermal effects to determine what fraction of the total torque is actually required by each bearing. Since both bearings rotate at precisely the same speed, the energy dissipated in each bearing is proportional to the torque generated by each bearing. The constants of proportionality are the same.

Figure 7 shows the simplified heat flow diagram of the outer housing. The top and bottom of the housing can be treated as insulated surfaces, because the plexiglas covers have a much higher thermal resistance than does the metal, or thin bakelite insulator. The bearings are also separated by a bakelite ring, which prevents large quantities of heat from flowing from one bearing directly to the other. As a first order approximation, the housing and the two races are assumed to be isothermal because of their extremely low thermal resistance. If the housing is thermally symmetric, then the ratio of the temperature difference between the test bearing and the housing, and the difference between the support bearing and the housing is exactly equal to the ratio of the test bearing torque to the support bearing torque. Knowing this ratio, and the sum of the torques, the test bearing torque can be determined. A more general treatment of this concept is contained in appendix A.

Motor torque is measured using a reaction torque sensor (fig. 1). The motor is suspended from the sensor, so that any torque applied to the drive pulley is counteracted by the sensor. The sensor is a strain gage type, so a conditioner/indicator is also used. The conditioner/indicator has an analog output, which is used to transmit data to the computer. Typical torque values are on the order of 0.071 N-m (10 in.-oz) and are accurate to ±0.0007 N-m (±0.1 in.-oz).

Temperatures are measured using thermistors, since they are more accurate than thermocouples at temperatures near room temperature. The thermistor resistances are measured using a Fluke 8520A Digital Multimeter (DMM) four-wire system, which, in principle, operates much like the LCZ meter four-wire system (two wires carry a known current, two wires carry back the resulting voltage drop), except that a direct current source is used, instead of the ac source used by LCZ meter. The DMM also communicates with the computer using the IEEE-488 interface bus.

In order for a single DMM to read the resistance of all four thermistors (test bearing, support bearing, outer housing, and ambient air temperatures), the leads have to be switched from one thermistor to the next. This is done with a relay box, using gold plated contact relays. It is important to use gold plated contact relays in good condition to keep the lead resistance to a

5

minimum. Other types of relays, or even gold plated contacts with a little
wear, produce variations in lead resistance, which show up as noise in the
temperature data.

The DMM leads pass through the same slip ring system as the LCZ meter to
get to the outer housing. Screw terminal connections are used to attach the
leads from the slip rings to the leads from the thermistors. Because of the
limited number of terminals on the slip ring assembly, it was necessary to
arrange the thermistors in a "Y" arrangement.

The thermal inertia of the bearing housing causes a time lag in the
response of the temperature readings to variations in torque. It was assumed
that the temperatures (K_i) are related to the bearing torques (T_i) through the
Laplace domain transformation:

$$G(s) = \frac{K_i(s)}{T_i(s)} = \frac{1}{\mathcal{T}s + 1} \qquad (2)$$

This is known as a first order lag. When a step change in torque occurs for
some reason, the temperature asymptotically approaches its new value according
to the governing equation, $T_i = C_1 e^{-(t/\mathcal{T})}$, where $\mathcal{T}$ is a response time con-
stant and C_1 is a general constant. It is possible to remove the time lag
from discrete data by applying the transformation:

$$Y_i = \frac{K_i - e^{-(t/\mathcal{T})}K_{i-1}}{1 - e^{-(t/\mathcal{T})}} \qquad . \qquad (3)$$

(See appendix A). Here the Y is the temperature with the time lag removed,
and $t = t_i - t_{i-1}$, where t represents the elapsed time. The subscript i
represents the value at the ith discrete value, and $\mathcal{T}$ is the response time
constant. This transformation is differential in nature, and thus, any noise
in the data is magnified. Actual values for $\mathcal{T}$ for the various thermistors
are determined from plots of temperature from runs where the bearing load was
abruptly changed, creating a step in the bearing torques.

EXAMPLES OF DATA

Figures 8 to 10 show examples of data generated with a super-refined gyro
bearing lubricant (SRG) using the above described instrumentation. Table I
contains typical physical property data for SRG 200. Table II lists the
bearing geometry and nominal operating parameters.

The figures show typical ranges, variations, and resolutions for the
different measured (conductance, capacitance, race and ball speeds, tempera-
tures and motor torque) and calculated values (film thickness, basic speed
ratio, and bearing torques). All plots were generated from a single test that
was run to failure. Failure occurred at approximately 18 000 sec.

6

CONCLUSIONS

A fully instrumented and automated bearing test rig now exists that can be used in the study of the failure of angular contact ball bearings running in the parched EHL regime. This real-life bearing test should give quantitative results indicating which factors are more significant in the failure sequence. This, in turn, should help in the synthesis of new lubricants and bearing materials and coatings, and provide valuable data for the design of systems which operate in the parched regime.

APPENDIX A

The test bearing torque can be viewed as the product of two quantities: the sum of the test and support bearing torques, T_Σ, and the fraction of that sum which goes to the test bearing, β_t. Mathematically these quantities are expressed as follows:

$$T_\Sigma = T_s + T_t \tag{1A}$$

$$\beta_t = T_t / T_\Sigma \tag{2A}$$

where:

T_t test bearing torque

T_s support bearing torque

T_Σ is found by measuring the torque output of the drive motor, multiplying by the ratio of pulley diameters to obtain the torque applied to the housing, and subtracting out losses due to slip ring friction and windage:

$$T_\Sigma = \frac{D_h T_m}{D_m} - T_L \tag{3A}$$

where:

T_m torque output by the motor

T_L torque lost to windage and slip ring friction

D_h diameter of housing pulley

D_m diameter of motor pulley

Losses due to windage can be shown to be on the order of the resolution of the motor torque sensor and are neglected in practice. Loss due to the slip ring friction is a constant, experimentally measured to be 0.0044 N-m (0.62 in.-oz).

To determine β_t, it is useful to define a new quantity η_t, the ratio of the support bearing to the test bearing torque. The ratio is related to β_t by the expression:

$$\beta_t = \frac{1}{1 + \eta_t} \tag{4A}$$

8

Since both bearings rotate at identical speeds,

$$\eta_t = \frac{\tau_s}{\tau_t} = \frac{Q_s/\Omega_s}{Q_t/\Omega_t} = \frac{Q_s}{Q_t} \qquad (5A)$$

where:

Q_s rate of heat dissipation by support bearing

Q_t rate of heat dissipation by test bearing

Ω_s support bearing speed

Ω_t test bearing speed

From this relationship it follows that:

$$\beta_t = \frac{Q_t}{Q_t + Q_s} \qquad (6A)$$

In the determination of β_t, it is convenient to think of the housing as a network of thermal resistances (fig. A1), and to draw on an analogy between heat transfer theory and electrical circuit theory. In this model, the thermal resistance of the bearing races and the metallic part of the housing are neglected, since their thermal conductances are two orders of magnitude higher than the plexiglass or bakelite parts, while the geometric dimensions of all the parts are similar. R_1 and R_2 represent the thermal resistance between the metallic part of the housing and the test and support bearing races, respectively. R_x represents the thermal resistance between the bearing races, while R_c represents the thermal resistance between the metallic part of the housing and ambient air. R_3 and R_4 are included in the model to account for other minor means of heat dissipation from the bearing races.

Ideally, $R_1 = R_2$, and R_3, R_4, and R_x would be infinite. In this case, Q_s and Q_t are given by

$$Q_s = \frac{T_s - T_h}{R_1} \qquad (7A)$$

$$Q_t = \frac{T_t - T_h}{R_1} \qquad (8A)$$

where:

T_t temperature of the test bearing race

T_s temperature of the support bearing race

T_h temperature of the metallic part of the housing

9

It follows that β_t is given by

$$\beta_t = \theta \qquad (9A)$$

where θ is the temperature difference ratio defined by:

$$\theta = \frac{T_t - T_h}{T_t + T_s - 2T_h} \qquad (10A)$$

Since the idealized case is not realized in practice, the more general case of figure A1, with all the R's finite and different is used to solve for β_t as a function of θ. A Taylor series expansion of the resulting expression yields the following polynomial in θ.

$$\beta_t = A + [1 + B + C] \cdot \left[\sum_{n=1}^{\infty} \theta^n D^{n-1}\right] \qquad (11A)$$

where:

$$A = \frac{(\lambda_2 - \lambda_1)(1 + \varepsilon_1)}{\left[1 + \lambda_2(2 + \varepsilon_2)\right](1 + \varepsilon_1) + \lambda_3(1 + \varepsilon_2)}$$

$$B = \frac{2\lambda_1(1 + \varepsilon_1) - \lambda_2(2 + 3\varepsilon_1 + \varepsilon_2 + \varepsilon_1\varepsilon_2) - \varepsilon_2\lambda_3 - \varepsilon_1}{\left[1 + \lambda_2(2 + \varepsilon_2)\right](1 + \varepsilon_1) + \lambda_3(1 + \varepsilon_2)}$$

$$C = \frac{(1 + \varepsilon_1)(\lambda_2 - \lambda_1)\left\{\varepsilon_1[1 + \lambda_2(2 + \varepsilon_2)] + \varepsilon_2\lambda_3\right\}}{\left\{[1 + \lambda_2(2 + \varepsilon_2)](1 + \varepsilon_1) + \lambda_3(1 + \varepsilon_2)\right\}^2}$$

$$D = \frac{\varepsilon_1\left[1 + \lambda_2(2 + \varepsilon_2)\right] + \varepsilon_2\lambda_3}{\left[1 + \lambda_2(2 + \varepsilon_2)\right](1 + \varepsilon_1) + \lambda_3(1 + \varepsilon_2)}$$

where:

$$\lambda_1 = R_2/R_x ; \quad \lambda_2 = R_c/R_3 ; \quad \text{and} \quad \lambda_3 = R_1/R_3$$

are the dimensionless "leakage parameters," and:

$$\varepsilon_1 = (R_1/R_2) - 1 ; \quad \text{and} \quad \varepsilon_2 = (R_3/R_4) - 1$$

are the dimensionless "asymmetry parameters." Under the idealistic assumptions given above ($R_1 = R_2$, and R_3, R_4, and R_x infinite), all the leakage parameters and asymmetry parameters are zero, and equation (11A) reduces to equation (9A). Under the more realistic set of assumptions that the leakage parameters and asymmetry parameters are nonzero, but small compared to unity, the following expression is obtained from equation (11A):

10

$$\beta_t = (\lambda_2 - \lambda_1) + \left[1 - 2(\lambda_2 - \lambda_1) - \epsilon_1\right]\theta + \epsilon_1\theta^2 \qquad (12A)$$

As expected, this expression is very similar to equation (9A), except for a small correction to the linear term, a small constant, and a small nonlinear term. A combination of theoretical and experimental considerations have shown that:

$$\lambda_2 - \lambda_1 < 0.03 \quad \text{and} \quad |\epsilon_1| < 0.02$$

Using these limits, the maximum error in using the simplified β_t equation (9A) is less than 9 percent. Therefore, equation (9A) was used for data analysis. Though this method is quite effective for steady state or slowly changing conditions, the thermal inertia of the housing makes the dynamic response of the system rather poor, with time constants on the order of 10 min. To deal with this problem, three new variables are introduced: Y_t, Y_s, and Y_h. These represent the values that the temperature T_t, T_s, and T_h, respectively would have if the thermal inertia of the system was negligible. Transformed into the Laplace domain, the actual temperatures are assumed to be related to these ideal temperatures by a transfer function $G_j(s)$ as follows:

$$T_j(s) = G_j(s)Y_j(s) \qquad (13A)$$

where s is the Laplace transform variable and j represents any of the indices t, s, or h. Furthermore, the transfer functions are assumed to be of the form:

$$G_j(s) = \frac{e^{-st_{o,j}}}{t_{c,j}S + 1} \qquad (14A)$$

This represents a simple first-order lag with time constant $t_{c,j}$, and dead time, $t_{o,j}$. Knowing the actual temperatures, the ideal temperatures can then be found from the expression:

$$Y_j(s) = \frac{T_j(s)}{G_j(s)} \qquad (15A)$$

Since the temperatures are not actually known as continuous functions of time, but rather as discrete data points, it is convenient to use a different transformation, much like the LaPlace transform, but known as the Z-transform and defined:

$$Z\left[f(k\overline{T})\right] = \sum_{k=0}^{N-1} f(k\overline{T})Z^{-k}$$

where:

N   number of data points

$\overline{T}$ time interval between points

k   an integer

The points are assumed to be taken at uniform intervals, $\overline{T}$. To determine the ideal temperatures, an analogy to equation (15A) is used in the Z-domain:

$$Y_j(z) = \frac{T_j(z)}{G_j(z)} \tag{17A}$$

Transforming equation (16A) into the Z-domain, and making use of the definition of the transform in equation (16A) yields the end result:

$$Y_j(t_i) = \frac{T_j(t_i) - T_j(t_{i-1})e^{-(t_i - t_{i-1})/t_{c,j}}}{1 - e^{-(t_i - t_{i-1})/t_{c,j}}} \tag{18A}$$

where t_i represents the time at which the ith temperature reading was taken. It can be shown equation (18A) is valid even if $t_i - t_{i-1}$ is not equal to $\overline{T}$.

The various time constants, $t_{c,j}$, and dead time constants, $t_{o,j}$, are determined experimentally by running the rig until the temperatures have reached a steady state, then creating a sudden change in the load applied to the bearing. A time constant is simply the time it takes for a temperature to reach 63.2 percent of its new steady state value, while the dead time constant is the time required for the temperature to begin responding after the application of the load step. In this case, $t_{c,t}$, and $t_{c,s}$ are found to be approximately 550 sec and $t_{c,h}$ to be 700 sec, while the dead time constants are substantially less than $\overline{T}$, and thus negligible.

Equation (18A) can be applied to the actual temperature data to obtain the temperatures that would have resulted if the system had negligible thermal inertia. These ideal temperatures can be substituted into equation (10A) in place of the actual temperatures to obtain a test bearing torque measurement with a much more rapid response time.

There is one notable drawback to this method of lag removal. Any noise in the data gets multiplied by a factor of $1 \big/ \left(1 - e^{-\overline{T}/t_{c,j}}\right)$. For a nominal sampling time of $\overline{T} = 20$ sec and a time constant of $t_{c,j} = 600$ sec, this means approximately a 30-fold increase in the noise. The torque values calculated from the resulting idealized temperature data tend to be so noisy that small effects are obliterated. This method of lag removal still has some merit for larger effects, however, and the experimentalist is left to choose between slow response and substantial noise in this effort to interpret the data.

12

REFERENCES

1. Wedeven, L.D.; Evans, W.; and Cameron, A.: Optical Analysis of Ball Bearing Starvation. J. Lubr. Technol., vol. 93, no. 3, July 1971, pp. 349-363.

2. Dowson, D.; and Higginson, G.R.: A Numerical Solution to the Elastohydrodynamic Problem. J. Mech. Eng. Sci., vol. 1, no. 1, June 1959, pp. 6-15.

3. Kingsbury, E.: Parched Elastohydrodynamic Lubrication. J. Tribology, vol. 107, no. 2, Apr. 1985, pp. 229-233.

4. Archibald, F.R.; and Blasingame, B.P.: The Jog Mechanism in Gyroscopes. Air, Space and Instruments, S. Lees, ed., McGraw-Hill, 1963, pp. 498-502.

5. Horsch, J.D.: Correlation of Gyro-Spin Axis Ball Bearing Performance with Dynamic Lubricating Films. ASLE Trans., vol. 6, no. 2, Apr. 1963, pp. 112-124.

6. Kingsbury, E.P.: Lubricant Breakdown in Instrument Ball Bearings. J. Lubr. Technol., vol. 100, no. 3, July 1978, pp. 386-394.

7. Kingsbury, E.P.: Pivoting and Slip in an Angular Contact Bearing. ASLE Trans., vol. 27, no. 3, July 1984, pp. 259-262.

8. Kannel, J.W.; and Dufrane, K.F.: Rolling Element Bearings in Space. 20th Aerospace Mechanics Symposium, NASA CP-2423, 1985, pp. 121-132.

9. Hunter, S.D.: Oil Film Thickness Measurement and Analysis for an Angular Contact Ball Bearing Operating in Parched Elastohydrodynamic Lubrication. NASA CR-179506, 1986.

10. Kingsbury, E.P.: Basic Speed Ratio of an Angular Contact Bearing. J. Lubr. Technol., vol. 102, no. 3, July 1980, pp. 391-394.

11. Tedeschi, F.P.: The Active Filter Handbook. TAB Books, Blue Ridge Summit, PA, 1979, pp. 227-241.

12. Dyson, A.; Naylor, H.; and Wilson, A. R.: The Measurement of Oil Films Thickness in Elastohydrodynamic Contacts. Elastohydrodynamic Lubrication, Proc. Inst. Mech. Eng. London, vol. 180, pt. 3B, 1966, pp. 119-134.

13. Allen, G.E.; Peacock, L.A.; and Rhoads, W.L.: Measurement of Lubricant Film Thickness in Hertzian Contacts. NASA CR-105378, 1968.

14. Dromgold, L.D.; and Klaus, E.E.: The Physical and Chemical Characteristics of an Homologous Series of Instrument Oils. Presented at 2nd Bearings Conference, Dartmouth College, Hanover, NH, Sept. 5, 1968.

TABLE I. - PHYSICAL PROPERTIES OF TEST LUBRICANT (SRG 200)

[Reference 14.]

Kinematic viscosity, CS	
at 38 °C	750
at 99 °C	42.2
Viscosity index	108
Pour point, °C	-7
Flash point, °C	288

TABLE II. - BEARING GEOMETRY AND OPERATING PARAMETERS

Bore, m	0.04
Ball diameter, m	7.9375×10^{-3}
Pitch diameter, m	5.40×10^{-2}
Contact angle, deg	12.7
Ball complement	21
Nominal load, N	891
Mean outer race stress, N/m^2	1.0×10^9
Mean inner race stress, N/m^2	1.2×10^9
Contact dimensions	
Outer semimajor axis, m	4.98×10^{-4}
Outer semiminor axis, m	1.22×10^{-4}
Inner semimajor axis, m	5.13×10^{-4}
Inner semiminor axis, m	1.04×10^{-4}
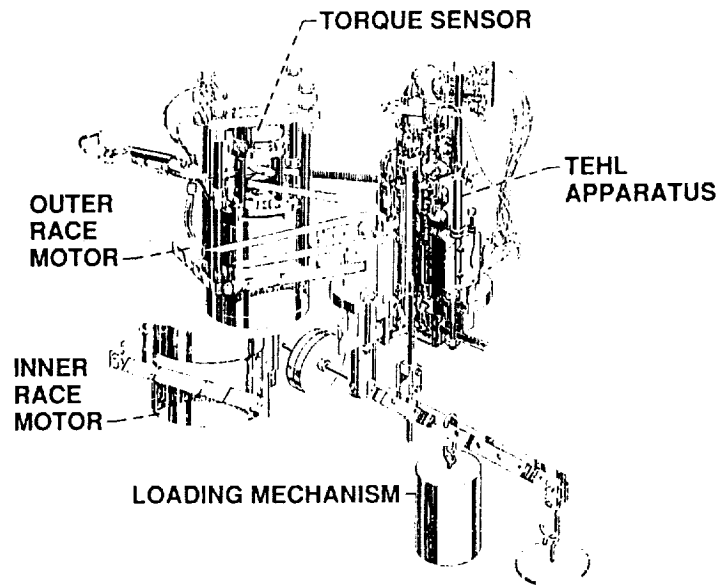
Figure 1.—Overall experimental apparatus.

TORQUE SENSOR

TEHL APPARATUS

OUTER RACE MOTOR

INNER RACE MOTOR

LOADING MECHANISM

Figure 2.—TEHL apparatus.

10 CHANNEL MAIN SLIP RING

2 CHANNEL INNER SLIP RING

TERMINAL BLOCK

OUTER RACE DRIVE GEAR

INNER RACE DRIVE GEAR

COIL ONE

COIL TWO

TEST BEARING

SUPPORT BEARING ONE

AMBIENT TEMPERATURE PROBE

SUPPORT BEARING TWO

SUPPORT BEARING THREE

SUPPORT BEARING FOUR

LOAD PIN

15
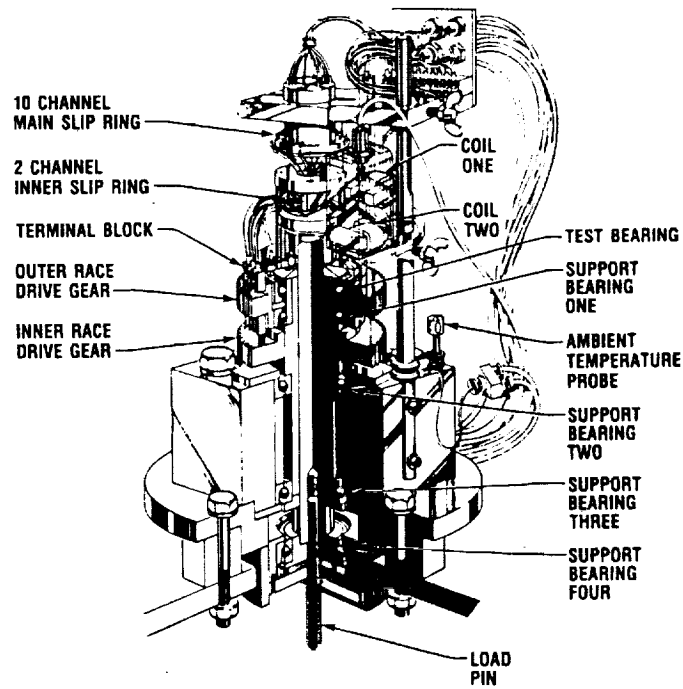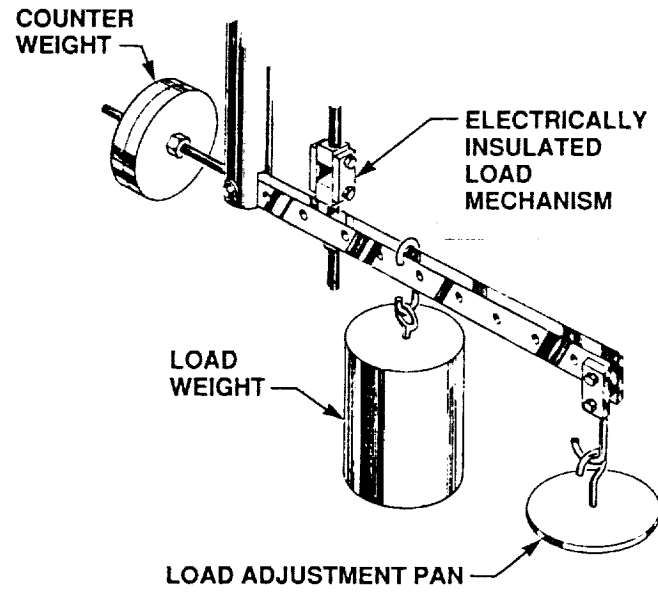
Figure 3.—Loading mechanism.

Note: $\Omega_i < 0$
$\Omega_o > 0$
$\Omega_b > 0$
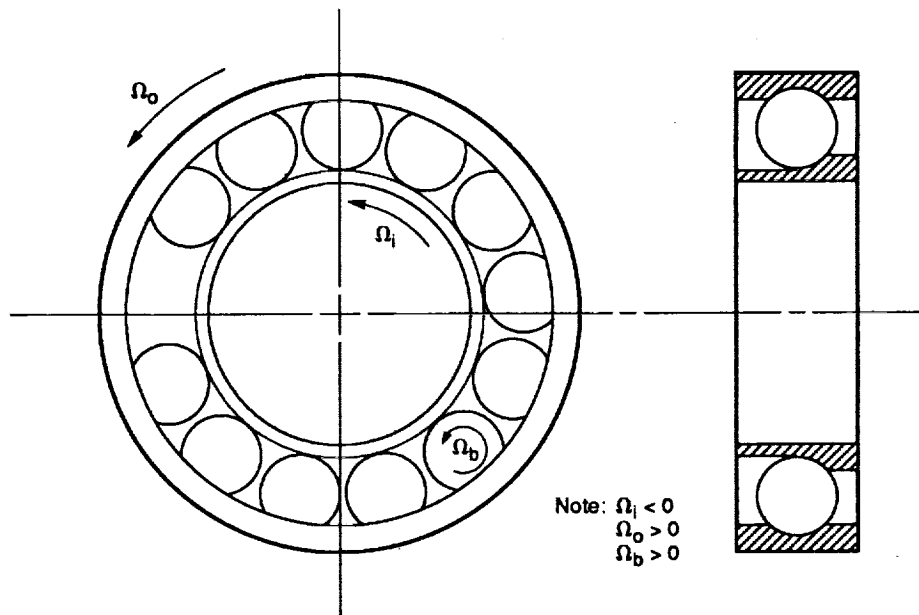
Figure 4.—Geometry of an angular contact ball bearing with a full ball complement.

16
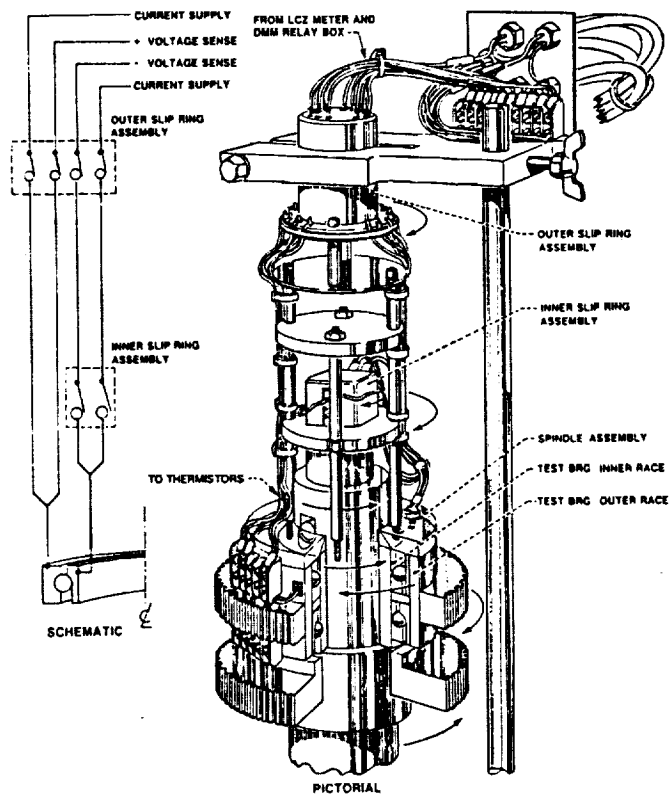
Figure 5.—Electrical connections–LCZ meter to test bearing.
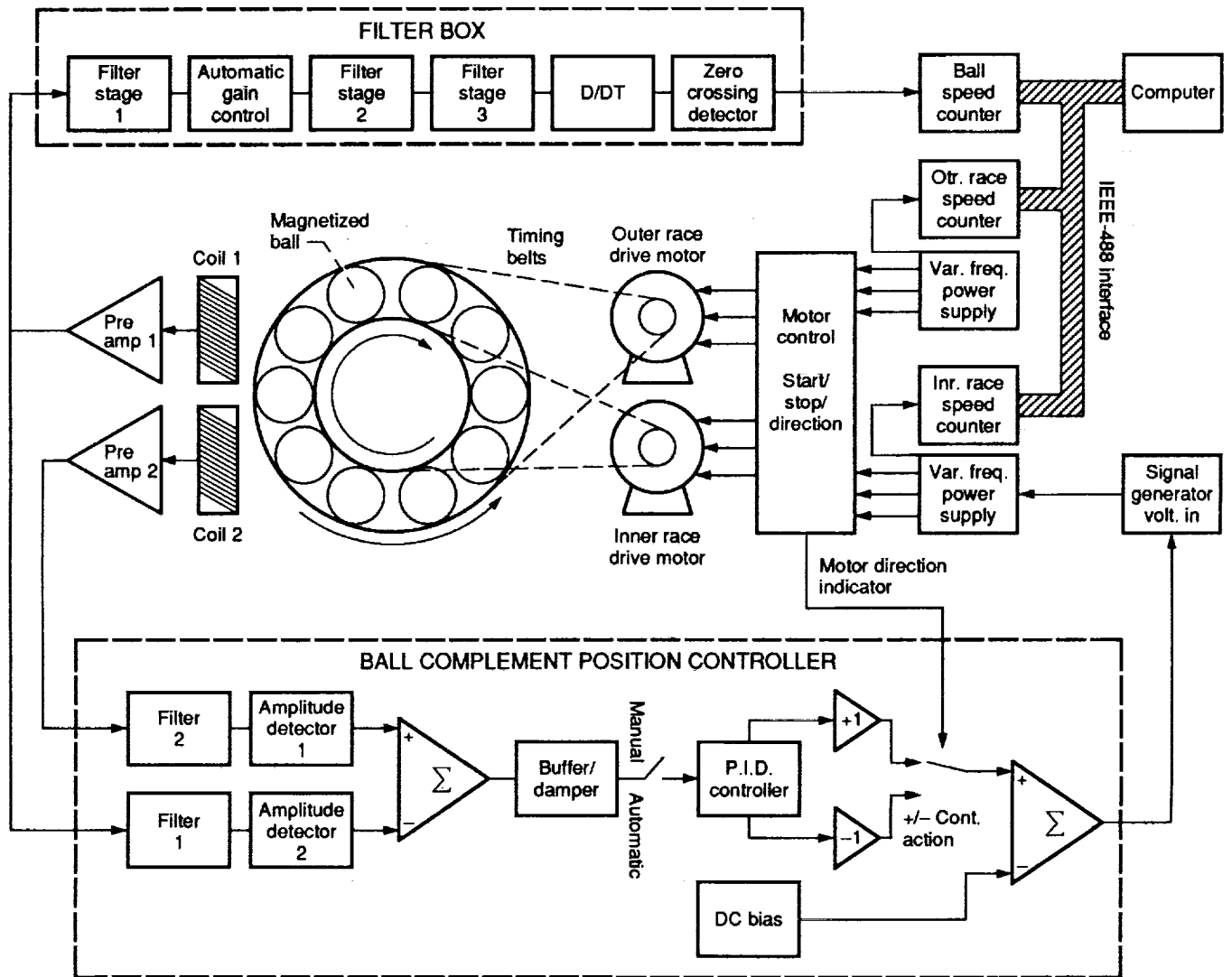
Figure 6.—Ball and race speed measuring system.
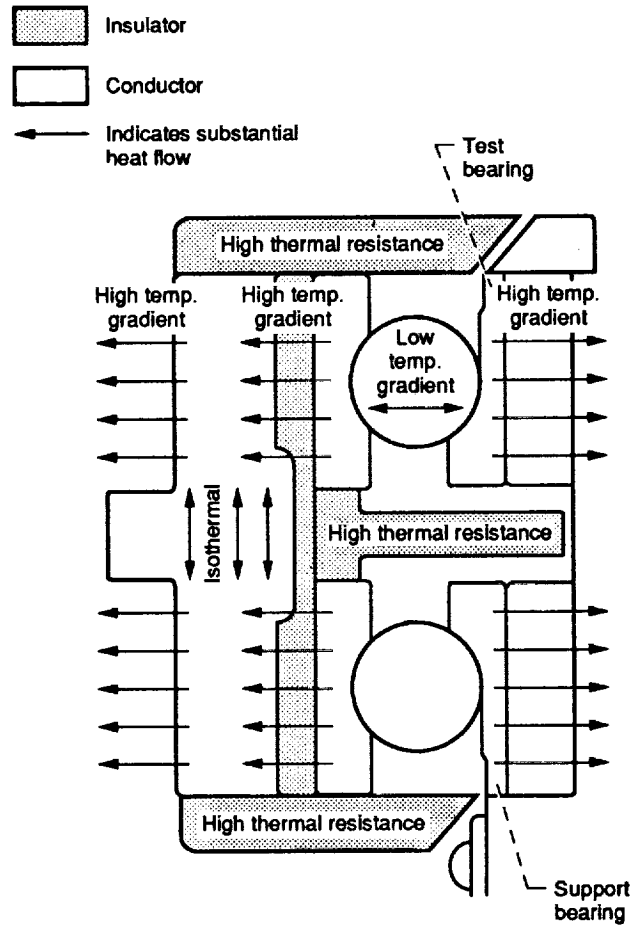
Figure 7.—Heat flow in outer housing.
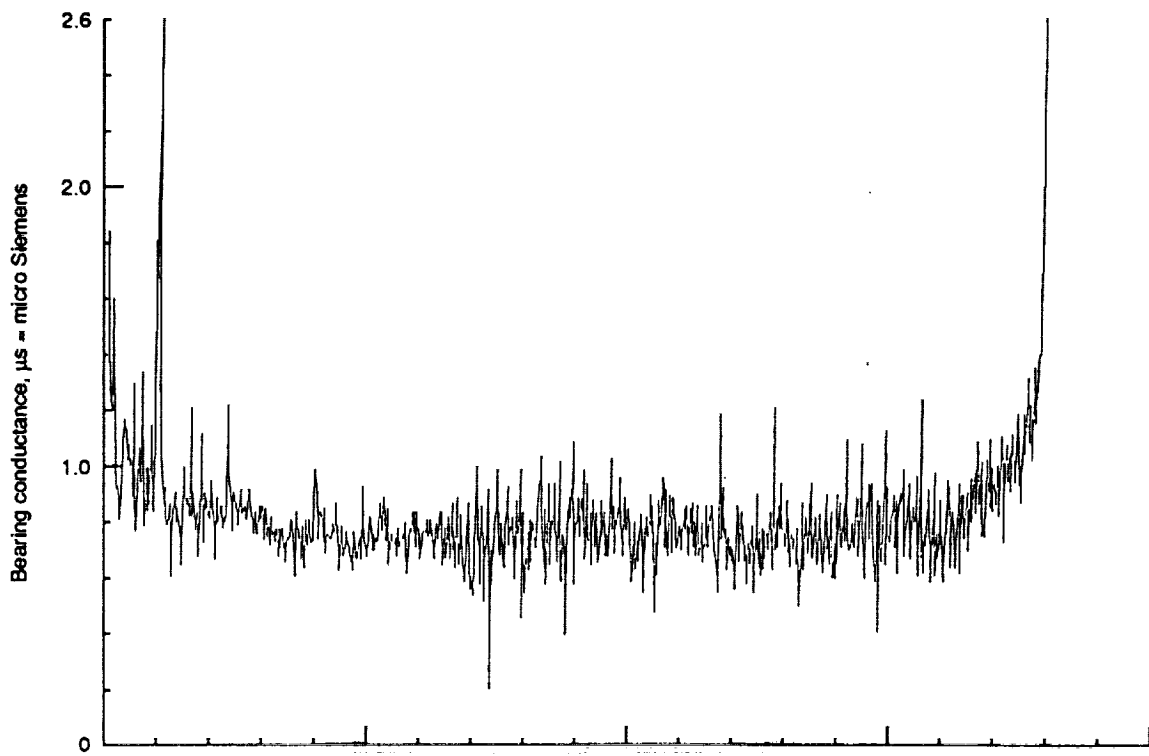
(a) Conductance across the bearing versus elapsed time. Bearing failure occurs at 18 000 seconds.
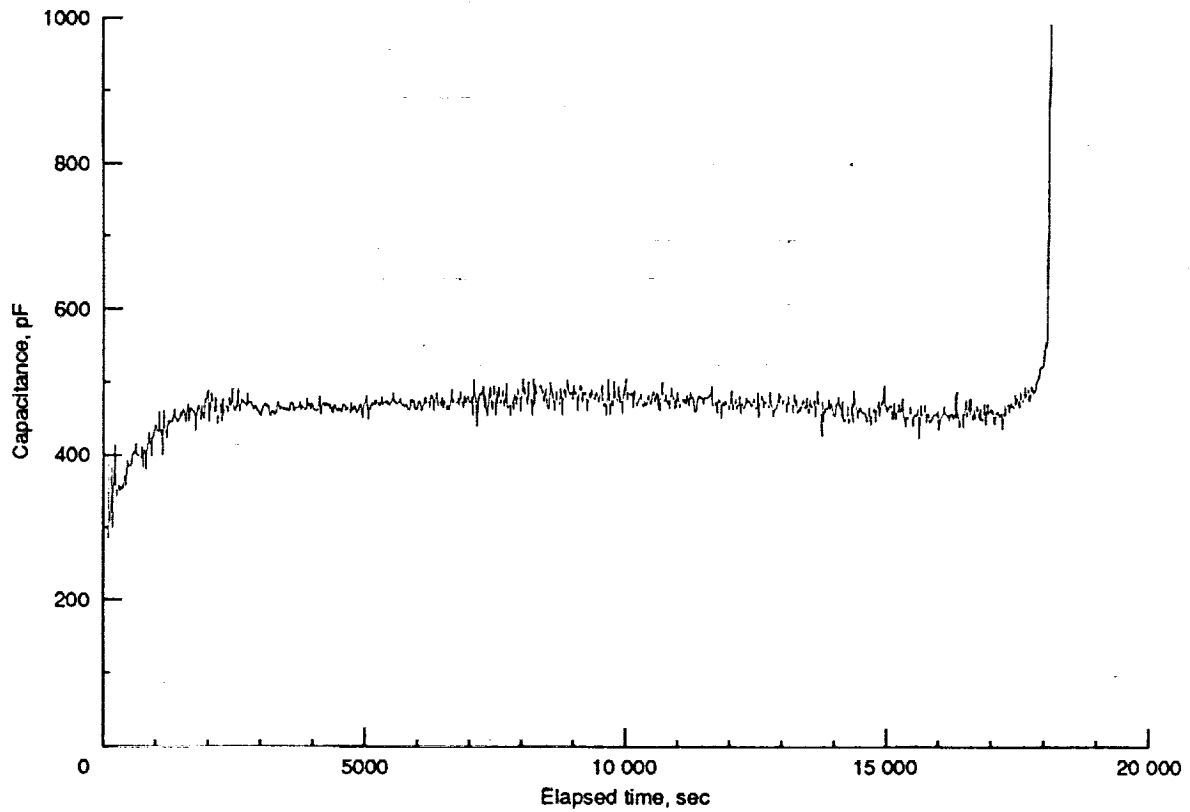
(b) Capacitance across the bearing versus elapsed time.

Figure 8.—Electrical measurements.
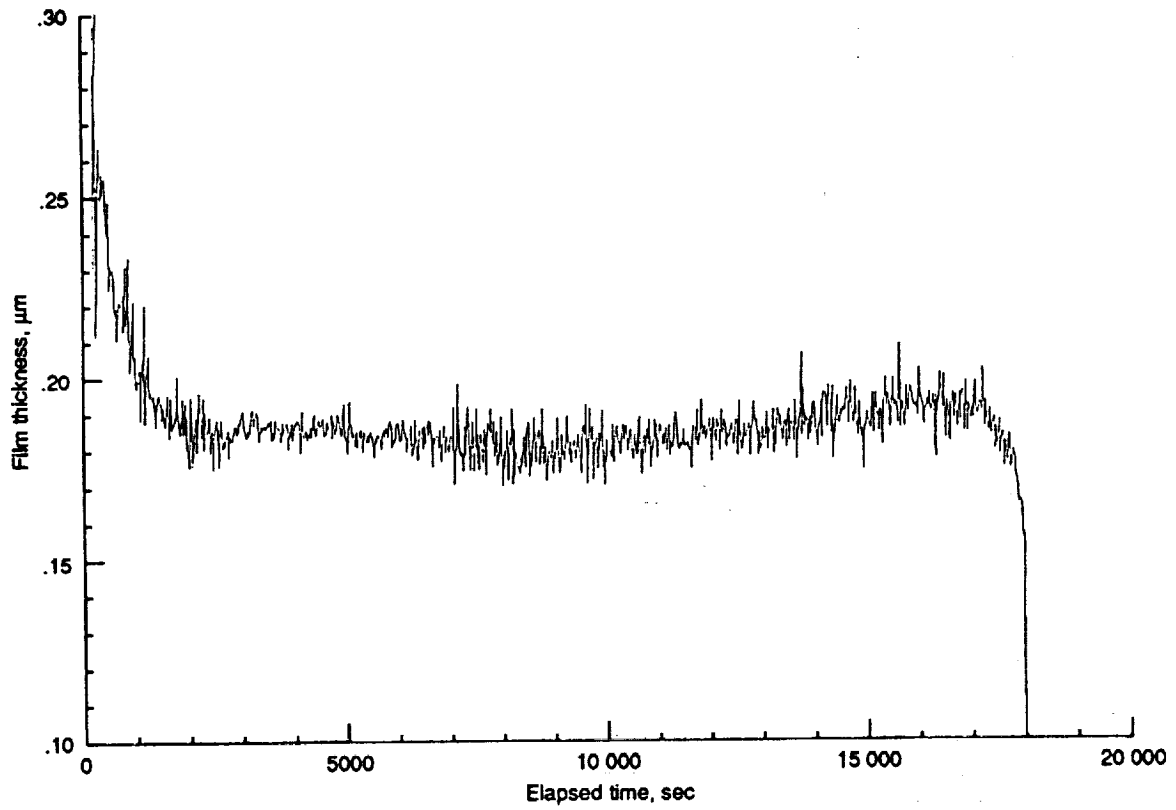
(c) Calculated film thickness versus elapsed time. Film thickness was calculated from capacitance data assuming smooth surfaces in the ball-race contact (no surface roughness).

Figure 8.—Concluded.
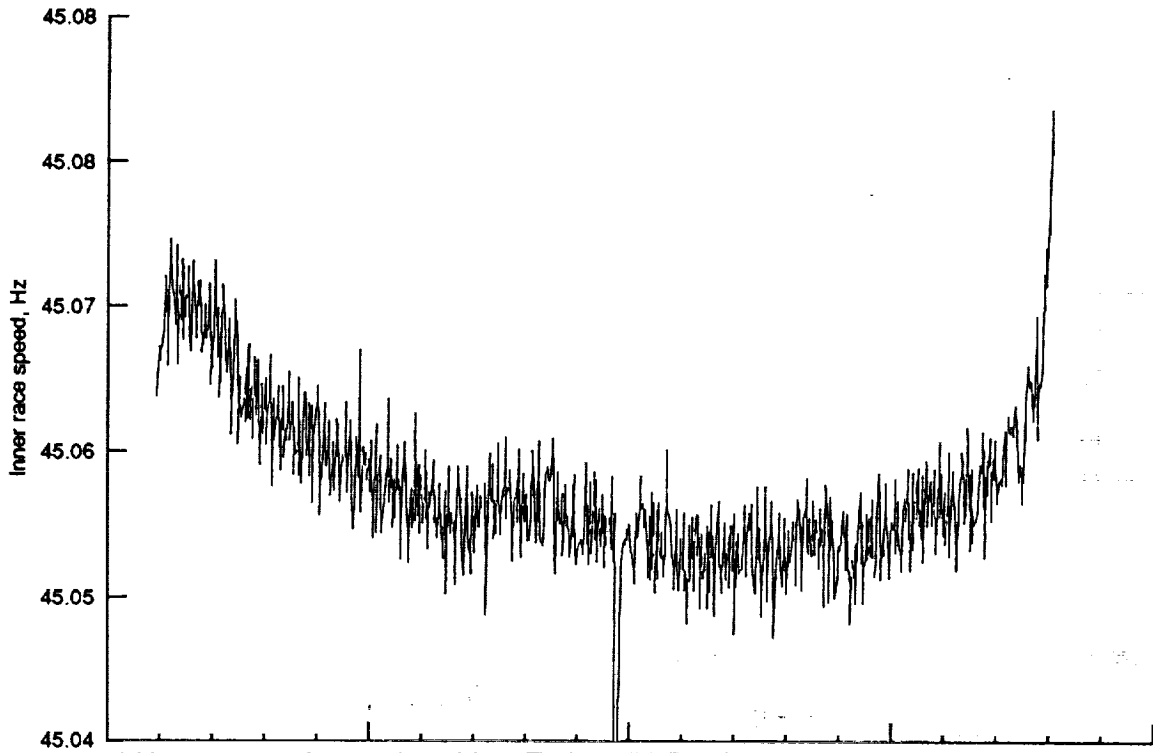
(a) Inner race speed versus elapsed time. The inner race speed is varied by the ball complement controller as required to keep the ball complement stationary.
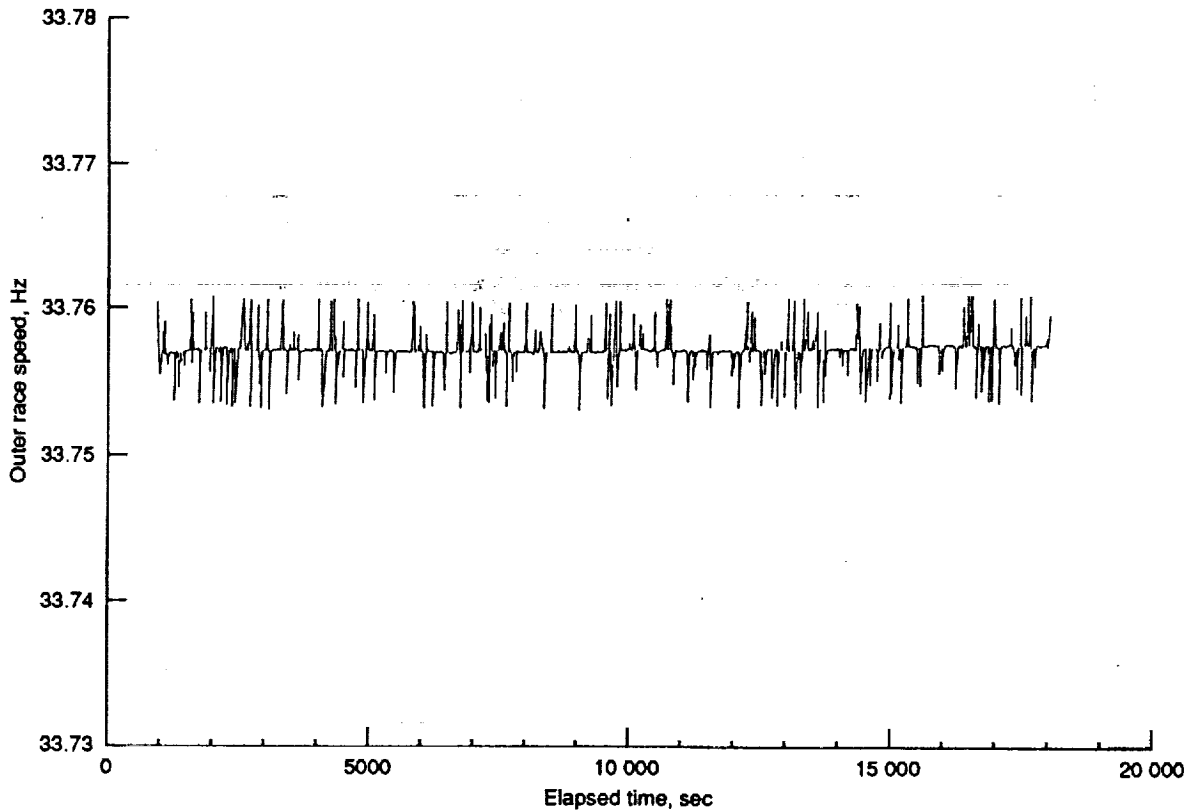
(b) Outer race speed versus elapsed time. The spikes are due to noise in the power supply oscillator causing frequency shifts.

Figure 9.—Speed measurements.

(c) Ball spin rate (spinning of the ball about its own axis) versus elapsed time.

(d) Basic speed ratio versus elapsed time.
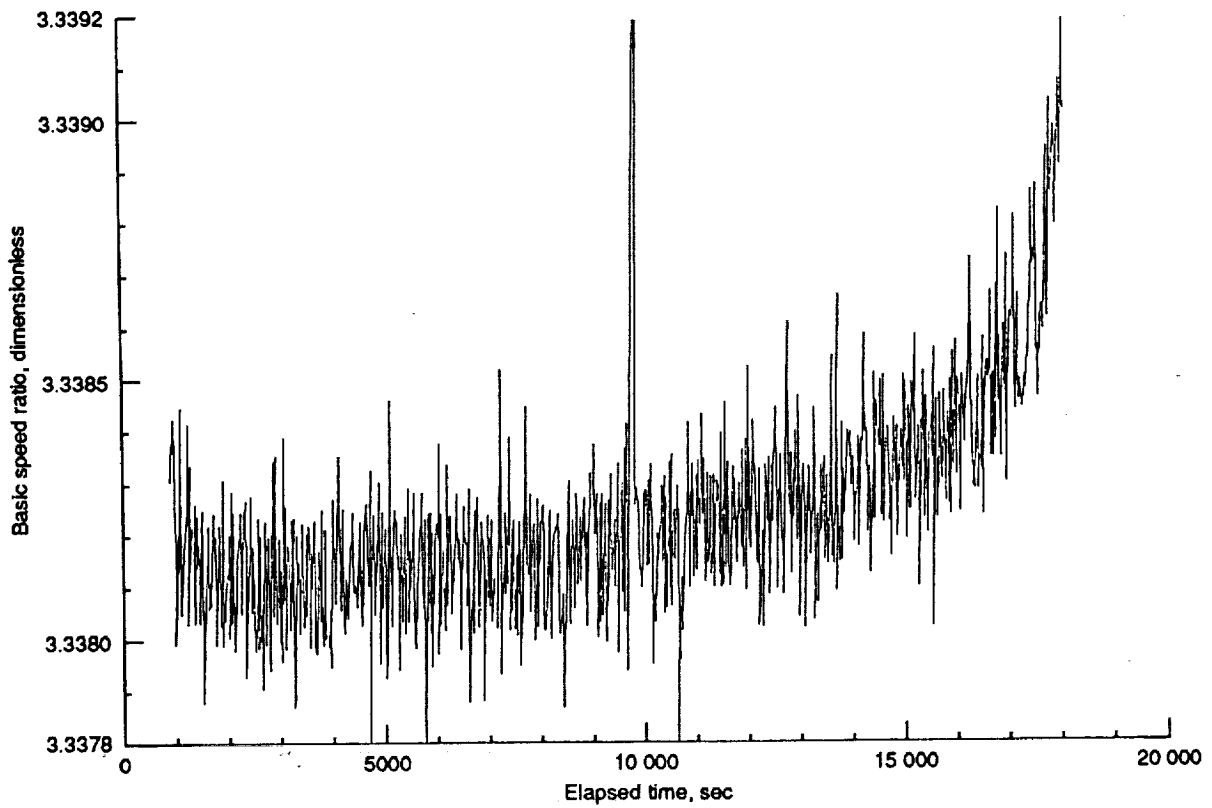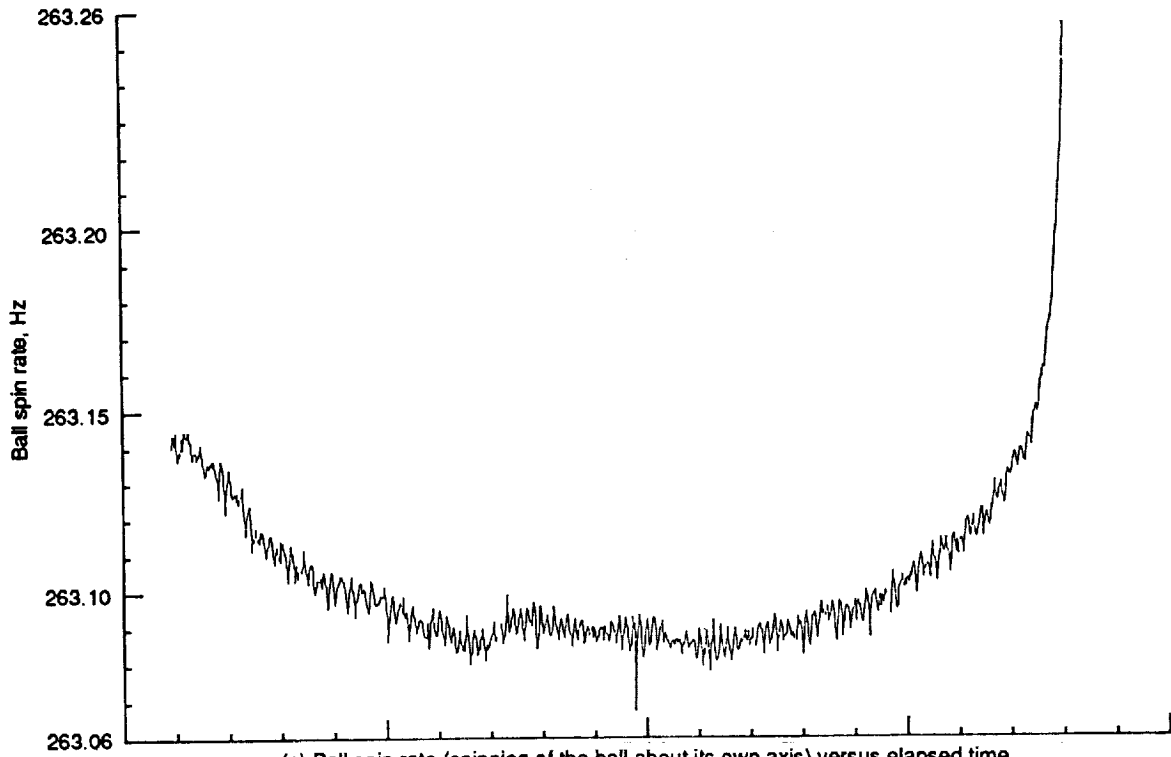
Figure 9.—Concluded.
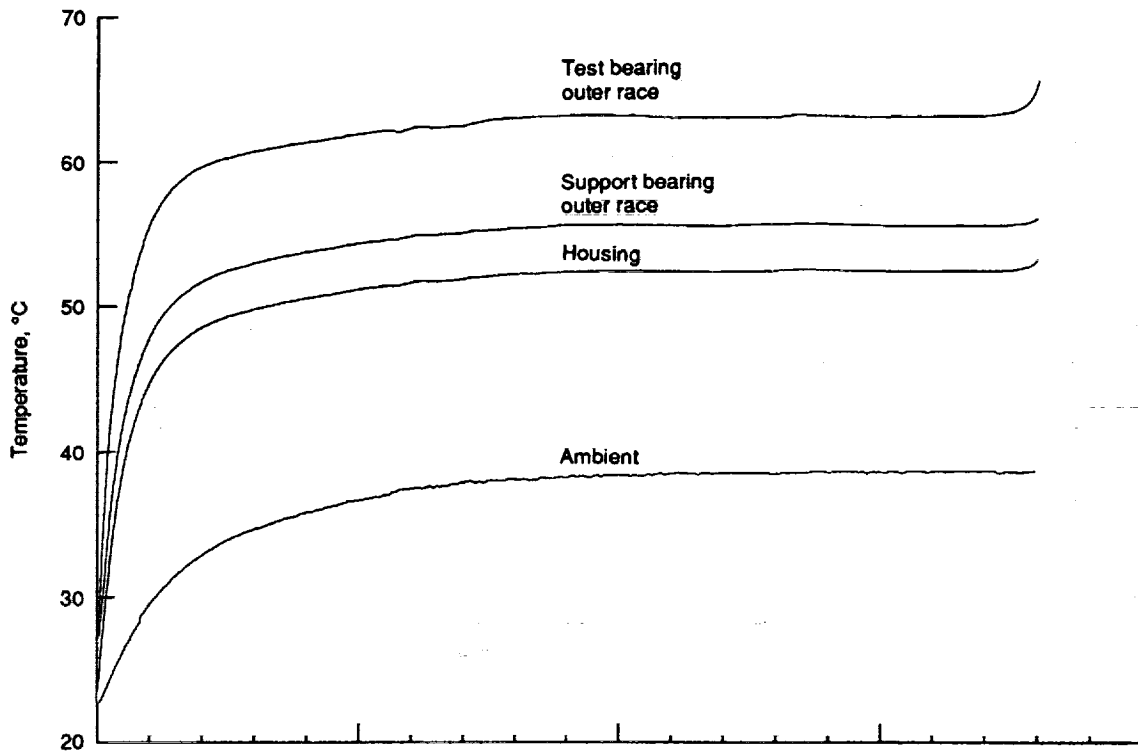
(a) Actual measured temperatures of various test rig components versus elapsed time.
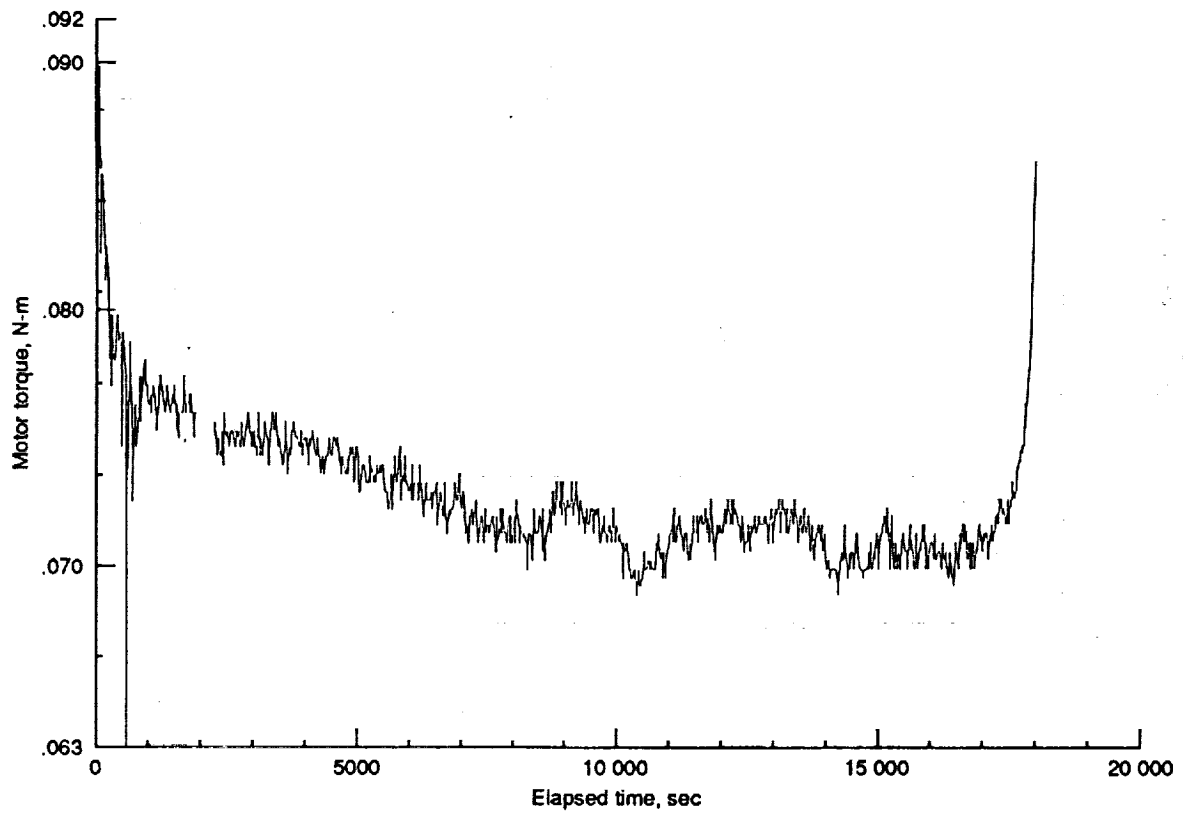
(b) Torque output of outer race drive motor versus elapsed time.

Figure 10.—Temperature and torque measurements.
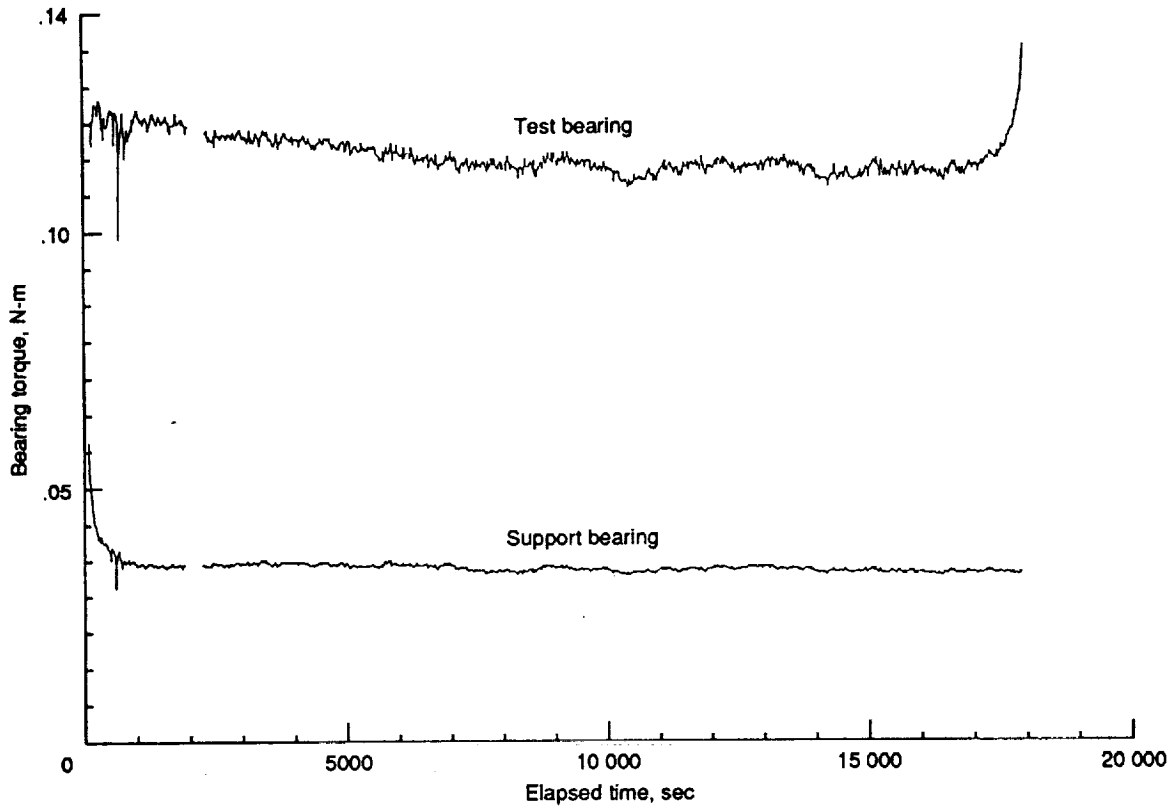
(c) Bearing torques calculated from motor torque and temperature data.

Figure 10.—Concluded.
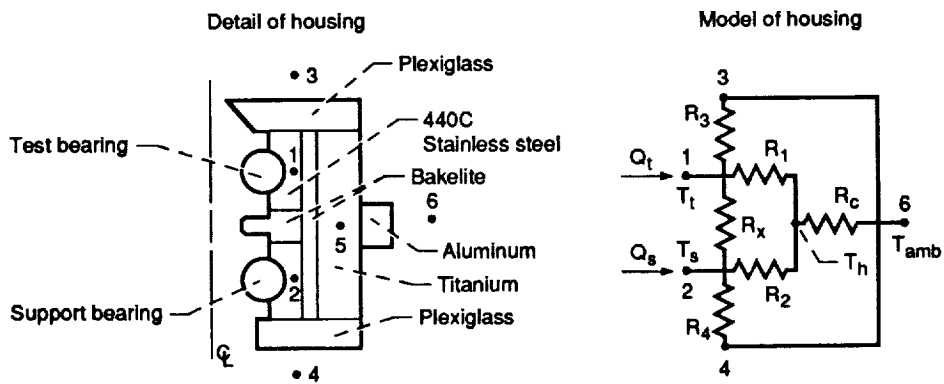
Figure A1.—Electrical analogy to heat transfer in bearing housing.

16. Abstract

A counter rotating bearing rig has been designed and constructed to study transient elastohydrodynamic lubrication phenomena. This paper describes new instrumentation and documents test procedures. Ball and race speed measurement systems and the capacitance (film thickness) measurement system were upgraded. Methods for measuring bearing torque and race temperatures were implemented.